Nanostructures, Semicrytalline Morphology, and Nanoscale Confinement Effect on the Crystallization Kinetics in Self-Organized Block Copolymer/Thermoset Blends

Qipeng Guo,*,† Ralf Thomann, and Wolfram Gronski*

Institut für Makromolekulare Chemie, Universität Freiburg, Stefan-Meier-Strasse 31, 79104 Freiburg, Germany

Rosina Staneva, Rouja Ivanova, and Bernd Stühn

Institut für Physik, Technische Universität Ilmenau, 98693 Ilmenau, Germany

Received January 6, 2003; Revised Manuscript Received February 27, 2003

ABSTRACT: This work reports the first instance of self-organized thermoset blends containing diblock copolymers with a crystallizable thermoset-immiscible block. Nanostructured thermoset blends of bisphenol A-type epoxy resin (ER) and a low-molecular-weight (M_n = 1400) amphiphilic polyethylene-*block*-poly(ethylene oxide) (EEO) symmetric diblock copolymer were prepared using 4,4′-methylenedianiline (MDA) as curing agent and were characterized by transmission electron microscopy (TEM), atomic force microscopy (AFM), small-angle X-ray scattering (SAXS), and differential scanning calorimetry (DSC). All the MDA-cured ER/EEO blends do not show macroscopic phase separation but exhibit microstructures. The ER selectively mixes with the epoxy-miscible PEO block in the EEO diblock copolymer whereas the crystallizable PE blocks that are immiscible with ER form separate microdomains at nanoscales in the blends. The PE crystals with size on nanoscales are formed and restricted within the individual spherical micelles in the nanostructured ER/EEO blends with EEO content up to 30 wt %. The spherical micelles are highly aggregated in the blends containing 40 and 50 wt % EEO. The PE dentritic crystallites exist in the blend containing 50 wt % EEO whereas the blends with even higher EEO content are completely volume-filled with PE spherulites. The semicrystalline microphase-separated lamellae in the symmetric EEO diblock copolymer are swollen in the blend with decreasing EEO content, followed by a structural transition to aggregated spherical micellar phase morphology and, eventually, spherical micellar phase morphology at the lowest EEO contents. Three morphological regimes are identified, corresponding precisely to the three regimes of crystallization kinetics of the PE blocks. The nanoscale confinement effect on the crystallization kinetics in nanostructured thermoset blends is revealed for the first time. This new phenomenon is explained on the basis of homogeneous nucleation controlled crystallization within nanoscale confined environments in the block copolymer/thermoset blends.

Introduction

Recent work from several laboratories has shown that the amphiphilic diblock copolymers are able to form well-defined ordered and disordered nanostructures in thermosetting epoxy resins[1−4] as well as in cross-linked phenolic resins.[5,6] In a previous study, we have successfully prepared self-organized nanostructured thermoset epoxy resin blends with amphiphilic triblock copolymers.[7] It has been shown that nanostructured thermoset blends can be obtained with block copolymers consisting of a thermoset-miscible block and a thermoset-immiscible block. However, all the thermoset-immiscible blocks of the block copolymers used by far are noncrystallizable amorphous polymers; no study has been done with the thermoset-immiscible blocks that are crystallizable. In self-organized thermoset blends with diblock copolymers consisting of a thermoset-miscible block and a crystallizable thermoset-immiscible block, the crystallizable thermoset-immiscible block will form separate microdomains at nanoscales within the nanostructured thermoset resins. It is envisaged that the crystallization, semicrystalline morphology, as well as the physical properties will be profoundly affected within the nanoscale confined environments. We will explore this topic in this work.

We report here nanostructured thermoset blends of epoxy resin and a low-molecular-weight polyethylene-*block*-poly(ethylene oxide) (PE−PEO) diblock copolymer. The PE−PEO diblock copolymer with 50 wt % ethylene oxide content and an average M_n = 1400, denoted as EEO throughout this paper, was used to prepare self-organized thermoset blends of varying compositions with a bisphenol A-type epoxy resin (ER) using 4,4′-methylenedianiline (MDA) as curing agent. It has been established in the previous studies that PEO homopolymer is miscible with aromatic diamine-cured ERs, including MDA-cured ER, owing to the favorable hydrogen-bonding interactions between the components.[8−10] The symmetric EEO diblock copolymer consists of an epoxy-miscible PEO block and an epoxy-immiscible PE block. The ER selectively mixes with the PEO block in the EEO block copolymer without dissolving the PE block, which thus leads to nanostructured thermoset blends. The crystallizable PE blocks that are immiscible with both ER and PEO blocks form separate microdomains on the nanoscales in the block copolymer/thermoset blends.

To our knowledge, this is the first instance of nanostructured thermoset blends containing diblock copolymers with a crystallizable thermoset-immiscible block.

* To whom correspondence should be addressed.
† Present address: Division of Chemical Engineering, The University of Queensland, Brisbane, QLD 4072, Australia. E-mail: q.guo@mailbox.uq.edu.au.

10.1021/ma0340154 CCC: $25.00
Published on Web 04/18/2003

The phase behavior, the nanostructures, crystallization, and the semicrystalline morphology in the cured materials are revealed by differential scanning calorimetry (DSC), transmission electron microscopy (TEM), atomic force microscopy (AFM), and small-angle X-ray scattering (SAXS). In particular, the nanoscale confinement effect on the crystallization kinetics in nanostructured thermoset blends is addressed for the first time.

Experimental Section

Materials and Preparation of Samples. The EEO diblock copolymer, namely, polyethylene-*block*-poly(ethylene glycol), was purchased from Aldrich Chemical Co., Inc. It had an average $M_n = 1400$ and 50 wt % ethylene oxide content. The uncured epoxy resin is the diglycidyl ether of bisphenol A (DGEBA) (Epikote 828 LV, Shell Chemicals) with an epoxide equivalent weight of 185. 4,4′-Methylenedianiline (MDA) (Aldrich Chemical Co., Inc.) was used as the curing agent. To prepare the MDA-cured ER/EEO blends, EEO was first dissolved in DGEBA with continuous stirring at 120 °C. The curing agent MDA was then added to the mixture at 110 °C with continuous stirring until a homogeneous ternary mixture was obtained. MDA was used in stoichiometric epoxide/amine ratios. The mixture was then immediately poured into an aluminum pan, degassed at 110 °C in a vacuum, and cured at 120 °C for 8 h, followed by postcuring successively at 150 °C for 1 h and 180 °C for 1 h.

Differential Scanning Calorimetry (DSC). The calorimetric measurements were made on a Perkin-Elmer Pyris 1 differential scanning calorimeter in a dry nitrogen atmosphere. Indium and tin standards were used for calibration for low and high-temperature regions, respectively. Samples of about 8 mg were placed in the DSC pan. All samples, except indicates otherwise, were first heated to +150 °C from −60 °C at a rate of 20 °C/min (first heating scan) and kept at that temperature for 2 min; subsequently they were cooled at a rate of −20 °C/min to detect crystallization (cooling scan). Following the cooling scan, a second scan was conducted at the same heating rate as the first. The midpoint of the slope change of the heat capacity plot of the second heating scan was taken as the glass transition temperature (T_g). The crystallization temperature (T_c) was taken as the minimum of the exothermic peak, whereas the melting temperature (T_m) was taken as the maximum of the endothermic peak.

Transmission Electron Microscopy (TEM). Samples were microtomed at −60 °C with a Leica EMFCS instrument equipped with a diamond knife. The resulting ultrathin sections of 80 nm thickness were picked up on copper grids and stained in the vapor of an aqueous solution of RuO_4. Stained samples were imaged in a LEO Omega 912 transmission electron microscope (TEM) with an accelerating voltage of 120 kV.

Atomic Force Microscopy (AFM). AFM experiments were performed with a Nanoscope III scanning probe microscope. The height and phase images were obtained simultaneously while operating the instrument in the tapping mode under ambient conditions. Images were taken at the fundamental resonance frequency of the Si cantilevers which was typically around 300 kHz. Typical scan speeds during recording were 0.3−1 line/s using scan heads with a maximum range of 16 × 16 μm. The phase images represent the variations of relative phase shifts, and are thus able to distinguish materials by their material properties. The flat surfaces of the blend samples used for examination were obtained by cutting with a Diatome diamond knife at −60 °C using a Leica EMFCS microtome.

Small-Angle X-ray Scattering (SAXS). The small-angle X-ray scattering (SAXS) experiments were performed with a Kratky compact camera (Anton Paar K. G., Graz, Austria) at room temperature. The Cu Kα radiation from a sealed X-ray tube was filtered with a nickel foil. The range of scattering vector $\mathbf{q} = (4\pi/\lambda)\sin(\theta/2)$, where $\lambda = 0.154$ nm is the wavelength and θ the scattering angle, was 0.06−5.4 nm^{-1}. The scattered intensity was recorded with a scintillation counter in a step-scanning mode. The sample of about 2 mm thickness was placed in a brass sample holder. The holder together with the collimation system was seated in an evacuated chamber. The background was corrected by subtraction of the scattering from an empty sample holder. The intensity was normalized to the incoming flux with the help of a moving slit device. The effect of the slitlike cross section of the beam was accounted for by desmearing the data using the standard procedure.[11]

Results and Discussion

Nanostructures, Semicrystalline Morphology, and Overall Phase Behavior. The MDA-cured ER/EEO blends were transparent with EEO content up to 40 wt %, but appeared translucent or opaque with 50 wt % or higher EEO content at room temperature due to the crystallization of EEO in the blends. All the blends were however transparent just above the melting point of EEO, indicating the absence of macroscopic phase separation. The morphology of the cured ER/EEO blends was investigated by TEM. The TEM micrographs of 95/5, 90/10, 80/20, 70/30, 60/40, and 50/50 cured ER/EEO blends are presented in Figure 1. The heterogeneous morphology at nanoscales was observed in all the cases. For the 95/5 ER/EEO blend, the spherical micelles with an average size in diameter of about 10 nm are dispersed in a continuous cured ER matrix (Figure 1a). The dark areas are PEO coronae because the PEO block was preferentially stained with RuO_4 compared to the core of the PE blocks and the cured ER matrix.[12] The TEM micrograph of 95/5 ER/EEO blend clearly shows a spherical micellar morphology. With increasing EEO content, the morphology of the cured blends changes gradually. The 90/10, 80/20 and 70/30 ER/EEO blends give rise to a similar morphology (Figure 1, parts b−d). The spherical PE micelles with a size of about 10 nm are dispersed in the continuous ER-rich microphase. The average distance between the neighboring spherical micelles decreases with increasing EEO content. DSC study (see below) shows that the PE blocks in the blend containing as less as 5 wt % EEO are still crystallized. The PE crystals with size on nanoscales are formed and restricted within the individual spherical micelles in the nanostructured ER/EEO blends with EEO content up to 30 wt %. For the blends containing 40 and 50 wt % EEO, spherical micelles are highly aggregated in a continuous ER-rich microphase. The TEM micrographs exhibit a morphology of aggregated spherical micelles with some characteristic of bicontinuous microphase structures (Figure 1, parts e and f). The size of the microphase structure is 10−15 nm.

Morphologies of the cured ER/EEO blends were also studied by AFM. The AFM images of cured ER/EEO blends clearly show microphase separation at nanoscales for various compositions (80/20, Figure 2a; 60/40, Figure 2b; 50/50, Figure 2c). For the 80/20 ER/EEO blend, the bright areas that are relatively stiff[13] are the ER-rich microphase whereas the dark areas are the PE-rich microphase (Figure 2a). It is clearly seen that the 80/20 ER/EEO blend exhibits spherical micellar morphology. The dark spherical PE microdomains with an average size in diameter of about 10−15 nm are dispersed in a bright continuous cured ER matrix. For the 60/40 and 50/50 ER/EEO blends (Figure 2, parts b and c), the bright areas are the ER-rich microphase composed of cross-linked ER network swollen with small amount of PEO blocks, the dark areas are the PE

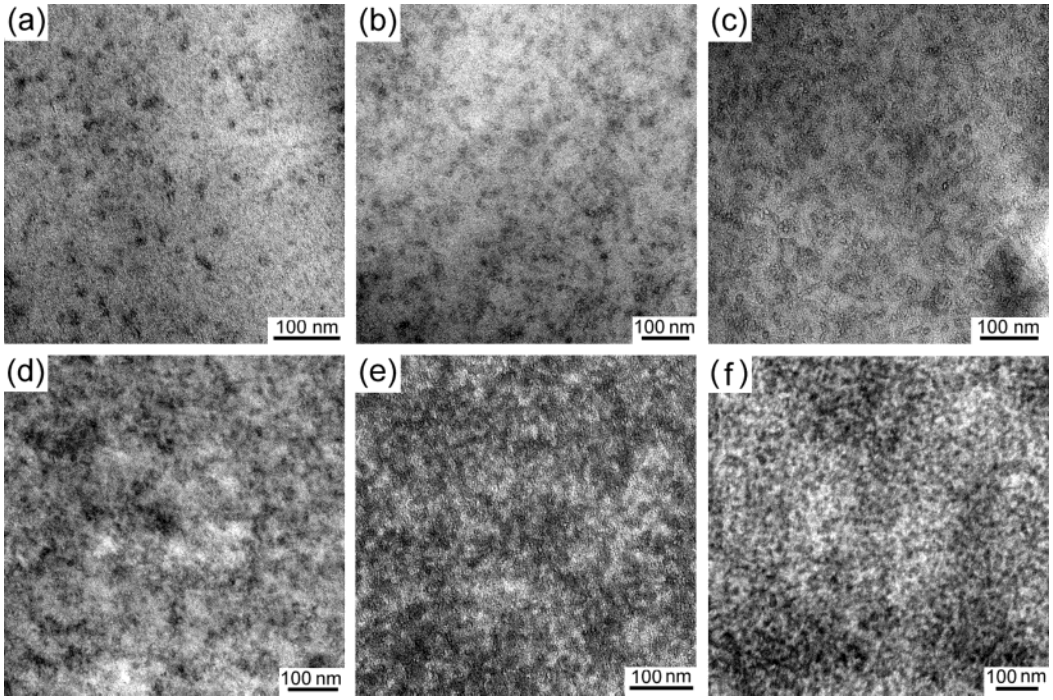

Figure 1. TEM micrographs of (a) 95/5, (b) 90/10, (c) 80/20, (d) 70/30, (e) 60/40, and (f) 50/50 MDA-cured ER/EEO blends. The specimens for TEM observation were stained with RuO_4.

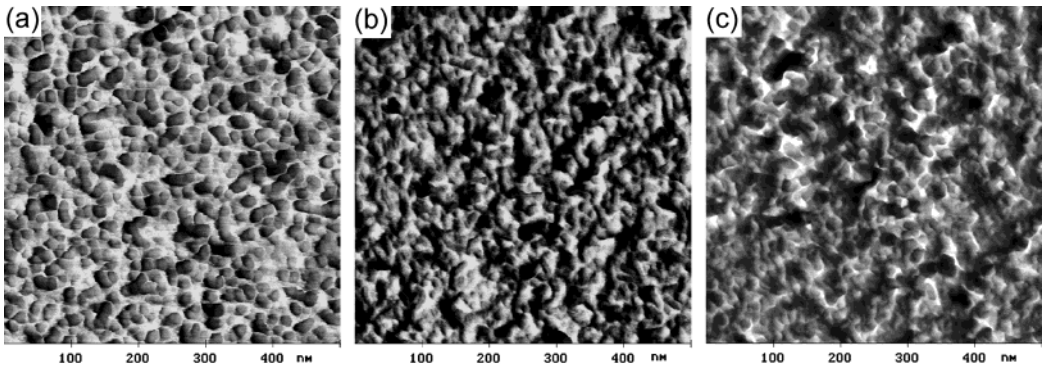

Figure 2. AFM phase images of (a) 80/20, (b) 60/40, and (c) 50/50 MDA-cured ER/EEO blends.

microdomains shielded by coronae of PEO blocks. The PE microdomains are relatively soft as the molecular weight of PE block is very low (only 700). The gray areas contain insufficiently cross-linked ER and more PEO blocks compared to the bright areas. The AFM observation clearly reveals a highly aggregated spherical micellar morphology with characteristic of bicontinuous microphase structures. These results are in agreement with the TEM observation (Figure 1, parts e and f).

The MDA-cured ER/EEO blends with 50 wt % or higher EEO content are semicrystalline. The 50/50 ER/EEO blend appeared translucent at room temperature but became clear at the temperatures above the melting point of EEO, implying that the blend was crystallized to some extent. The semicrystalline morphology of the 50/50 ER/EEO blend was examined also by TEM but at a much lower magnification. Figure 3a shows a TEM micrograph of PE dentritic crystallites observed in the 50/50 ER/EEO blend at the lower magnification. The PE blocks which are crystallizable and immiscible with both ER and PEO blocks formed a separate microphase in the thermoset blend and resulted in dentritic crystallites with size of 2−5 μm in diameter. Parts b and c of Figure 3 respectively show AFM height and phase images for the 50/50 ER/EEO blend; the images were obtained at a much higher magnification than the TEM micrograph in Figure 3a but still at a much lower magnification than the AFM image in Figure 2c. Although it is not easy to discern the semcrystalline morphology, the AFM phase image (Figure 3c) clearly displays a uniform, nanostructured phase morphology with some bicontinuous characteristic arising from highly aggregated spherical micelles.

Spherulites were revealed in the 38/62 ER/EEO blend by the TEM study. The blend was volume-filled with spherulites with size of 10−30 μm in diameter. Figure 4a displays a TEM micrograph taken from the inside region of a PE spherulite for 38/62 ER/EEO blend, clearly displaying PE crystalline lamellae. The epoxy/PEO matrix is stained dark with RuO_4. The TEM study shows that the 25/75 ER/EEO blend was also volume-filled with spherulites and the size of spherulites is 10−30 μm in diameter. Figure 4b presents a TEM micrograph within a PE spherulite in the 25/75 ER/EEO blend; the PE crystalline lamellae are clearly seen. Furthermore, TEM micrograph in Figure 4c clearly displays PE crystalline lamellae in the 18/82 ER/EEO blend. PE crystalline lamellae in the blends gradually

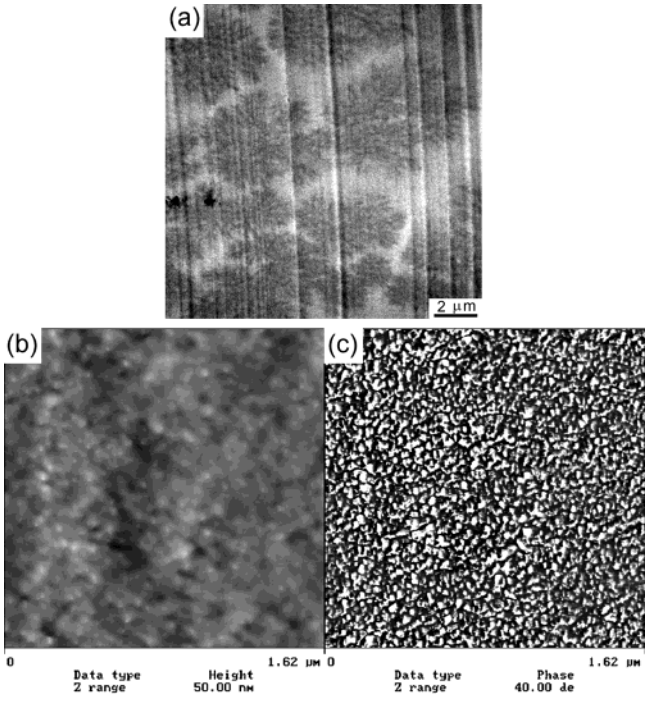

Figure 3. Semicystalline morphology of 50/50 MDA-cured ER/EEO blend at low magnifications. (a) TEM micrograph, (b) AFM height image, and (c) AFM phase image. The specimen for TEM observation was stained with RuO_4.

become more regular and less tilted with increasing EEO content from 62 to 82 wt %. Parts a and b of Figure 5 show TEM micrographs between the spherulite edge and the interspherulitic boundary region for 38/62 and 25/75 ER/EEO blends, respectively. The dark portion is within the crystalline spherulite whereas the bright portion is within the amorphous interspherulitic boundary region. It is evident that the spherical micellar morphology exists in the amorphous interspherulitic boundary regions for both 38/62 and 25/75 cured ER/EEO blends.

The TEM micrographs in Figures 4b and 5b also reveal that the 25/75 ER/EEO blend exhibits a networklike phase structure, i.e., the existence of a skeletal phase (the black network areas) which clearly displays characteristics of three-dimensional continuity with the size of the phase structure on the order of 50−100 nm. This networklike, skeletal phase structure is interwoven with PE crystalline lamellae within the spherulites. The networklike skeletal phase which looks black can be considered to be mainly composed of insufficiently cured ER molecules which are preferentially stained with RuO_4. To conform this, we used poly(hydroxyether of bisphenol A) (phenoxy) as a reference and found that RuO_4 preferentially stained phenoxy rather than the EEO diblock copolymer. Phenoxy is the corresponding linear high-molecular-weight homopolymer of the bisphenol A-type ER and has a structure similar to that of the insufficiently cured ER. It should be pointed out that, for the blend with EEO content as high as 75 wt %, the curing reaction could hardly be completed owing to the diluent effect and only highly branched ER molecules formed. It is interesting to see that the 25/75 ER/EEO blend is hierarchically nanostructured. The blend displays structural inhomogeneity, i.e., microphase-separated at two different nanoscales. The existence of hierarchical nanostructures has been reported previously in self-organized thermoset blends of ER with amphiphilic PEO−poly(propylene oxide)−PEO triblock copolymers.[7] In the present case for the 25/75 ER/EEO blend, the existence of structural inhomogeneity at two nanoscales can be accounted for by the evolution of the phase behavior during the curing process. The curing reaction between DGEBA and MDA resulted in the formation of highly branched ER molecules and imperfectly cross-linked ER network which then partially separated out from the EEO-rich phase to form a networklike, skeletal ER-rich phase with a size of 50−100 nm. This nanoscale phase separation caused the structural inhomogeneity on the order of 50−100 nm. Because of unfavorable interactions of PE blocks with PEO blocks as well as with the ER matrix, microphase separation further took place within the EEO-rich phase, bringing about the PE crystalline lamellae. Figure 5c presents an AFM phase image for 25/75 ER/EEO blend between the crystalline spherulite edge and the amorphous interspherulitic boundary region, clearly displaying a separate microphase (the black area). The black area has a much lower stiffness because it is mainly composed of insufficiently cured ER molecules.

SAXS measurements have been performed for samples of the plain EEO and the ER/EEO blends to characterize their microstructures. Desmeared SAXS patterns for the plain EEO at room temperature and at elevated temperatures are shown in Figure 6. At room temperature (25 °C), the main peak of the plain EEO diblock copolymer is located at a value of the scattering vector **q** corresponding to a long spacing of 11.6 nm. There is a second-order reflection clearly visible at double angular position of this first-order maximum. Such a sequence is characteristic of an arrangement of lamellae. The EEO diblock copolymer is microphase-separated into a lamellar structure with a long period of 11.6 nm corresponding to the spacing between neighboring

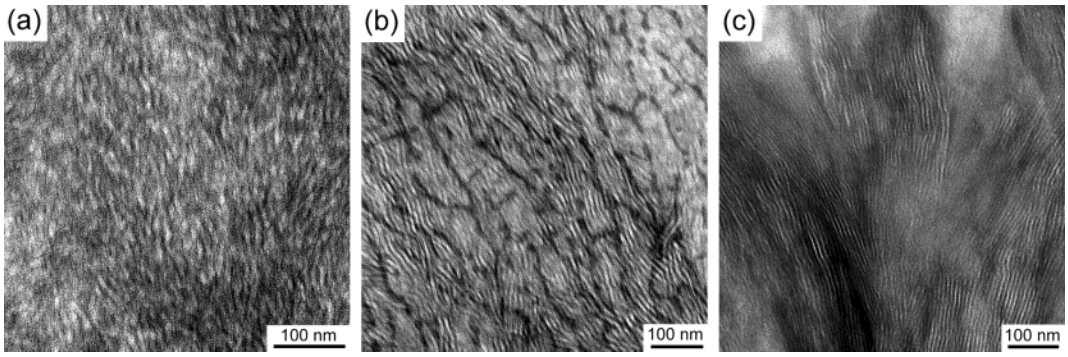

Figure 4. TEM micrographs showing semicrystalline morphology for (a) 38/62, (b) 25/75, and (c) 18/82 MDA-cured ER/EEO blends. The specimens for TEM observation were stained with RuO_4. The PE crystalline lamellae are clearly seen.

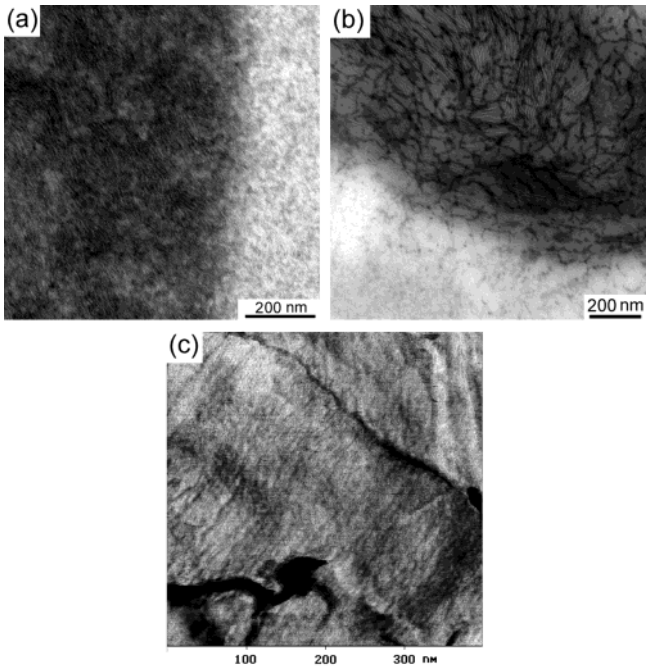

Figure 5. Morphology in the interspherulitic boundary regions for 38/62 and 25/75 MDA-cured ER/EEO blends. (a) TEM micrograph of 38/62 ER/EEO blend, (b) TEM micrograph of 25/75 ER/EEO blend, and (c) AFM phase image of 25/75 ER/EEO blend. The specimens for TEM observation were stained with RuO_4.

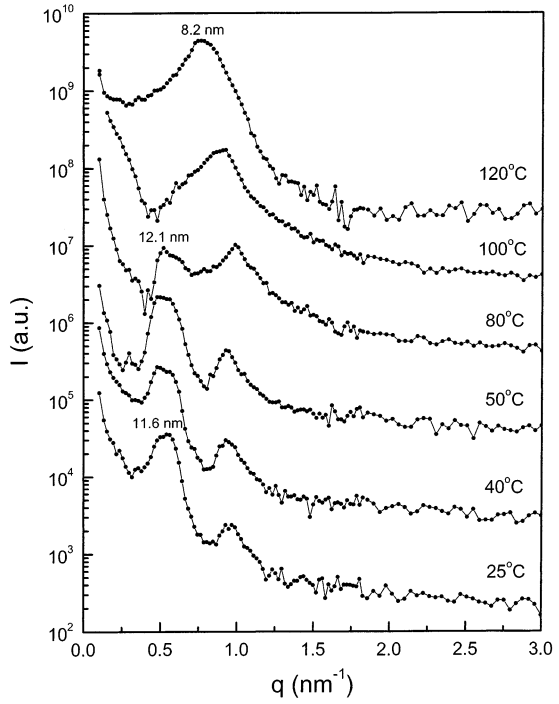

Figure 6. Desmeared SAXS patterns of the EEO diblock copolymer at different temperatures. The scattering vector **q** $= (4\pi/\lambda)\sin(\theta/2)$, where $\lambda = 0.154$ nm is the wavelength and θ the scattering angle.

lamellar regions of PE and PEO blocks; both PE and PEO are semicrystalline within the corresponding lamellar regions. As the molecular weight of EEO is very low, only single chain crystals can exist in each PE or PEO phase-separated lamellar region. Similar SAXS scattering patterns are observed for the EEO copolymer at 40, 50, and 80 °C. The EEO copolymer remains a lamellar structure at these temperatures. It is interesting to see that the low **q** peak is not well-defined and exhibits characteristic of a double peak. It can be seen from Figure 6 that there appears a shoulder at the left-side of the peak maximum at 25 °C. This shoulder corresponding to a long spacing of 12.1 nm becomes the maximum of the peak at 40, 50, and 80 °C; however the peak corresponding to the long spacing of 11.6 nm remains discernible at the elevated temperatures. The appearance of the double peak indicates the existence of two long spacings in the EEO copolymer, i.e., 11.6 and 12.1 nm, which may be caused respectively by the tilted and perpendicular arrangements of the PEO single stems related to the interfacial layers. Increasing temperature results in the melting of the crystalline PEO lamellae, accompanied by a transition from the tilted to perpendicular arrangements of the PEO stems related to the layers. It is also noted that once the PE blocks have melted a new scattering peak appears at the high q value which starts to grow gradually from 80 °C at the expense of the low **q** peak as the specimen is heated. This high **q** peak corresponds to a long spacing of 8.2 nm at 120 °C. Extinction of the low **q** peak coincides with the gradual PE melting from 80 to 120 °C. The melting of the crystalline PE lamellae leads in principle into a microphase-separated lamellar structure of amorphous PEO and PE blocks. However the SAXS peak shifts to larger **q** and broadens considerably, indicating the transition in practice into the disordered state of the diblock copolymer. The previous study by Hillmyer and Bates[14] has shown that there exists an order−disorder transition (ODT) at 110 °C for symmetric PE−PEO diblock copolymer win $M_n = 2100$. It is reasonable to believe that the ODT for the EEO diblock copolymer ($M_n = 1400$) in this study is occurring together or immediately following the melting of the PE blocks (106 °C by DSC). The SAXS results presented here for the pure EEO sample are in accordance with the small-angle neutron scattering results at a variety of temperatures obtained by Hillmyer and Bates (14) for the symmetric PE−PEO diblock copolymer with $M_n = 2100$.

Figure 7 shows desmeared SAXS patterns for the plain EEO and the ER/EEO blends at room temperature (25 °C). As discussed above, the pure EEO diblock copolymer at room temperature exhibits a semicrystalline microphase-separated lamellar structure with long spacing of 11.6 nm. However, the SAXS investigation for the blends only provides clear information in the limit cases of large and small volume fraction of EEO. The heterogeneous microstructures between give rise to the superposition of scattering patterns. For the 25/75 ER/EEO blend, long spacing is increased to be 15.0 nm indicating that the semicrystalline microphase-separated lamellae were swollen with the ER, i.e., insufficiently cured ER molecules. The amorphous insufficiently cured ER molecules mix with the epoxy-miscible PEO blocks to form a microphase layer of increased thickness between the semicrystalline PE lamellar regions whereas the thickness of the semicrystalline region of phase-separated PE blocks remained almost unaffected with the addition of the ER. This result is in agreement with the TEM observation. The 30/70 and 38/62 ER/EEO blends are not easily characterized as the main peaks in the SAXS patterns are less well-defined. However they contain PE crystalline lamellae as revealed by the TEM study. The appearance of

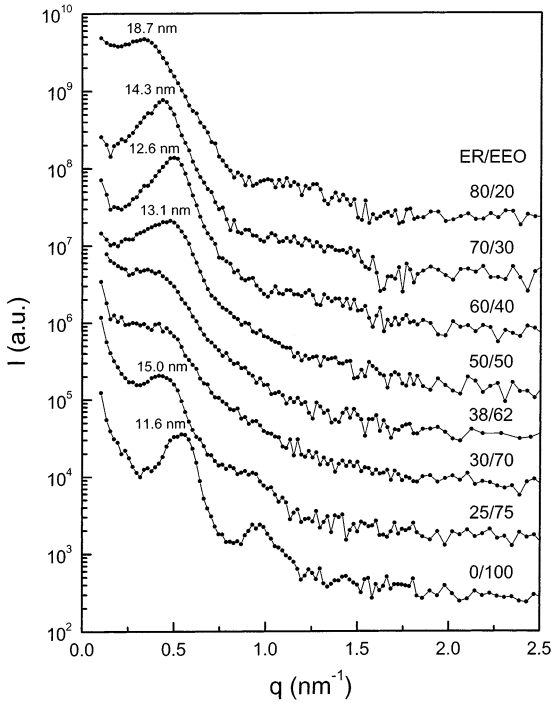

Figure 7. Desmeared SAXS patterns of MDA-cured ER/EEO blends at room temperature (25 °C). The scattering vector **q** = $(4\pi/\lambda)\sin(\theta/2)$, where $\lambda = 0.154$ nm is the wavelength and θ the scattering angle.

complicated main peaks can be attributed to the existence of spherical micelles in the amorphous interspherulitic boundary regions in these blends. These main peaks can be considered as the superposition of scattering patterns from the heterogeneous microstructures.

The 50/50 ER/EEO blend displays a well-defined scattering peak, but shifted to a higher q value indicative of some form of structural transition. Also, the main peak has broadened noticeably and its width is consistent with disorder, i.e., it resembles correlation hole scattering from disordered block copolymer.[15,16] The main peak for this blend appears at a q value corresponding to distance of 13.1 nm in real space, which is the size of the microphase structure, in accordance with the TEM result that is on the order of about 10−15 nm. This value can be considered to be the average distance between the neighboring spherical micelles. The spherical micelles in the 50/50 ER/EEO blend are highly aggregated and the microphase structure exhibits some characteristic of bicontinuity as revealed by the TEM and AFM images shown in Figures 1 and 2.

For the blends containing 40−20 wt % EEO, the scattering is from spherical micelles (or aggregated spherical micelles). With increasing EEO content from 20 to 40 wt %, the position of the scattering peak, i.e., the value of the scattering vector **q**, gradually increases, corresponding to a decrease of long spacing in real space from 18.7 to 12.6 nm as indicated in Figure 7. The average distance between the neighboring spherical micelles decreases with increasing EEO content, consistent with the TEM observation (Figure 1). For the 60/40 ER/EEO blend, the scattering can also be considered to be dominantly from highly aggregated spherical micelles. The main peak for the 60/40 blend appears at q value corresponding to distance in real space of 12.6 nm which is the size of the microphase structure, in agreement with the TEM result.

To obtain quantitative information on the spherical micelle size and distribution, the SAXS data for the blends containing 20−50 wt % EEO were fitted to the Percus−Yevick model for a liquidlike packing of spheres with hard-core interactions.[17−20] The intensity of scattering at a given scattering wavevector, $I(\mathbf{q})$, depends on the square of the contrast difference, $\Delta\rho^2$, the number of scattering particles, N, the shape and size of the scattering particle described by the form factor, $P(\mathbf{q})$, and interparticle correlations accounted for by a structure factor, $S(\mathbf{q})$:

$$I(\mathbf{q}) = \Delta\rho^2 N P(\mathbf{q}) S(\mathbf{q}) + background \qquad (1)$$

In modeling the scattering from the ER/EEO blends, we assume the PEO corona chains have essentially the same scattering density as the epoxy matrix (i.e., they are contrast-matched), so that scattering arises almost entirely from the contrast between the spherical PE micelle cores and the PEO/epoxy matrix. The scattering from these ER/EEO blends with spherical micellar morphology can be represented by the spherical form factor[21] convoluted with a Gaussian distribution with a standard deviation of σ to account for polydispersity in the micelle radii:

$$P(\mathbf{q},R_c,\sigma) = \int_0^\infty \frac{1}{\sigma\sqrt{2\pi}}\exp\left(\frac{-(R-R_c)^2}{2\sigma^2}\right) {v_0}^2 \times \left[\frac{3[\sin(qR_c) - qR_c\cos(qR_c)]}{(qR_c)^3}\right]^2 dR \qquad (2)$$

where R_c is the radius of the spherical-micelle core formed by the PE block and v_o is the volume of the sphere ($v_o = {}^4/_3\pi R_c^3$).

The interparticle correlations can be modeled as hard-sphere potentials between micelles with disordered (liquidlike) packing in a matrix. The direct correlation between two hard spheres was first described by Ornstein and Zernike,[22] and it was further approximated by Percus and Yevick[23] using a function with an analytical solution. The resulting expression, called the Percus−Yevick model, is

$$S(\mathbf{q},R_{hs},\phi) = \frac{1}{\left(1 + \frac{24\phi J(A)}{A}\right)} \qquad (3)$$

$$J(A) = \frac{\alpha}{A^2}(\sin A - A\cos A) + \frac{\beta}{A^3}[2A\sin A + (2 - A^2)\cos A - 2] + \frac{\gamma}{A^5}\{-A^4\cos A + 4[(3A^2 - 6)\cos A + (A^3 - 6A)\sin A + 6]\} \qquad (4)$$

$$\alpha = \frac{(1+2\phi)^2}{(1-\phi)^4};\ \beta = \frac{-6\phi(1+\phi/2)^2}{(1-\phi)^4};\ \gamma = \frac{\phi(1+2\phi)^2}{2(1-\phi)^4} \qquad (5)$$

where $A = 2\mathbf{q}R_{hs}$, with R_{hs} equal to the effective hard-sphere radius and ϕ being the effective volume fraction of spheres.[18,21] For the present system, R_c relates directly to the size of the PE core, whereas R_{hs} and ϕ are related to the size and volume fraction of the core and corona together. The intensity is modeled with eq 1 with $P(\mathbf{q})$ given in eq 2 and $S(\mathbf{q})$ given in eq 3. The contrast factor N and v_o are independent of **q** and were

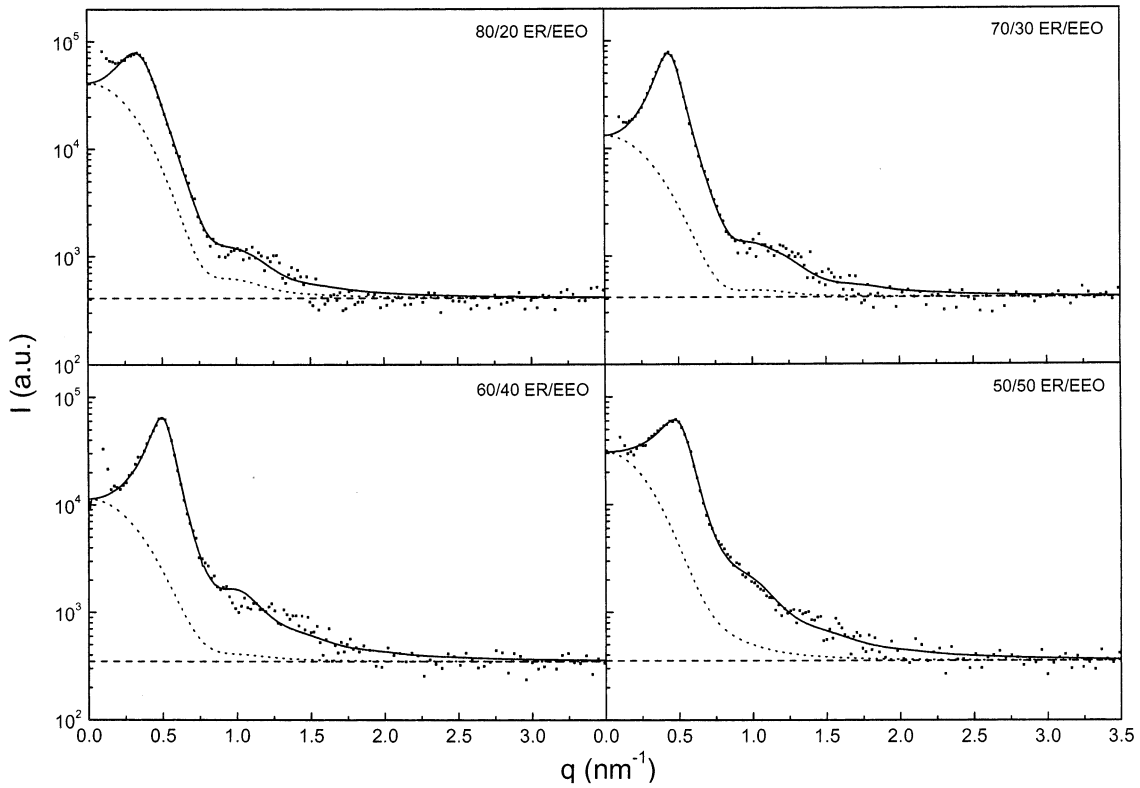

Figure 8. Percus−Yevick fits to four SAXS data taken from Figure 7. The full line is simulated scattering with the Percus−Yevick model for liquidlike packing of spheres with eq 1. The dashed line is the background which is constant for a given sample. The dotted line is the form factor of spheres simulated with eq 2.

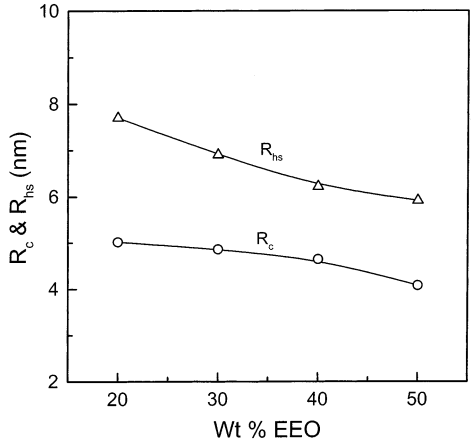

Figure 9. R_c and R_{hs} obtained from the Percus−Yevick fits as a function of the EEO diblock copolymer content.

combined into a single prefactor to fit the SAXS data. Figure 8 shows Percus−Yevick fits to the SAXS data for 80/20, 70/30, 60/40, and 50/50 ER/EEO blends. The full lines are the scatterings simulated with the Percus−Yevick model with eq 1, fitting the SAXS data very well for all the four blends. The background is constant for a given sample as represented by the dashed lines. The form factors of spheres simulated with eq 2 are represented by the dotted lines. Values for R_c, R_{hs}, σ, and ϕ can be obtained from the Percus−Yevick fits in Figure 8. Figure 9 shows R_c and R_{hs} values obtained as a function of the EEO diblock copolymer content. The sizes of the PE core in diameter ($2R_c$) are between 8 and 10 nm whereas those of whole the spherical micelle (the core and corona together) in diameter ($2R_{hs}$) are between 12 and 16 nm, in good agreement with the TEM observation. R_c remains nearly constant which is characteristic of spherical micelles, whereas R_{hs} remarkably decreases with increasing EEO content. This result demonstrates that the addition of the EEO copolymer produces more spherical micelles of nearly the same size.

The values of the effective volume fraction ϕ obtained from the Percus−Yevick fits are 0.17, 0.33, 0.37, and 0.30 for 80/20, 70/30, 60/40, and 50/50 ER/EEO blends, respectively. The ϕ value increases accordingly with EEO content up to 40 wt %. However, the ϕ value drops to 0.30 for 50/50 ER/EEO blend. It should be pointed out that the spherical micelles are highly aggregated in the 50/50 ER/EEO blend and the Percus−Yevick model is not the exact one for this case.

From the results presented above, we can clarify the overall phase behavior of the MDA-cured ER/EEO blends. The plain EEO exhibits a semicrystalline microphase-separated lamellar morphology. The lamellae are swollen in the blend with decreasing EEO content down to 62 wt % followed by a structural transition to aggregated spherical micelles that exhibit some characteristic of bicontinuous microphase structure (50 and 40 wt % EEO), and eventually spherical micelles at the lowest EEO contents (30−5 wt % EEO).

Miscibility, Melting Behavior, and Nanoscale Confinement Effect on the Crystallization Kinetics. Miscible blends containing at least one crystallizable component have attracted considerable interest. In contrast, little attention has been paid to miscible or even partially miscible blends of thermosetting resins with a crystallizable linear polymer.[8] From a consideration of thermodynamics, an increase in the molecular weight of either of the components of a miscible blend should reduce the entropy of mixing. Consequently, macroscopic phase separation induced by cross-linking

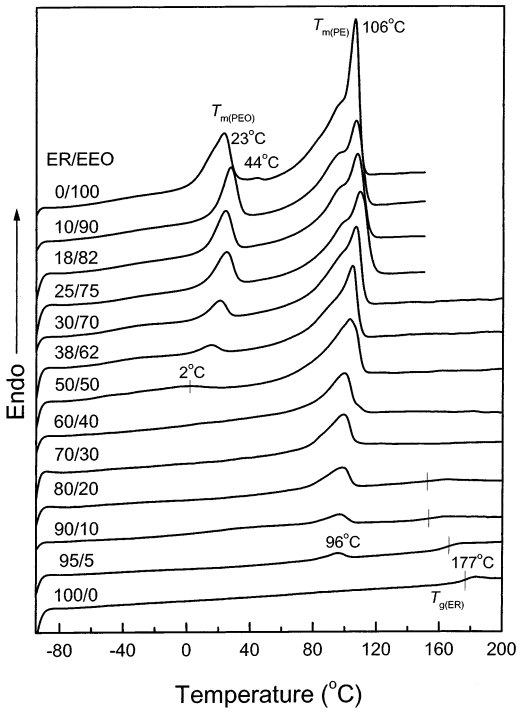

Figure 10. DSC thermograms of the second scan of the MDA-cured ER/EEO blends after the cooling scan. The heating rate is 20 °C/min.

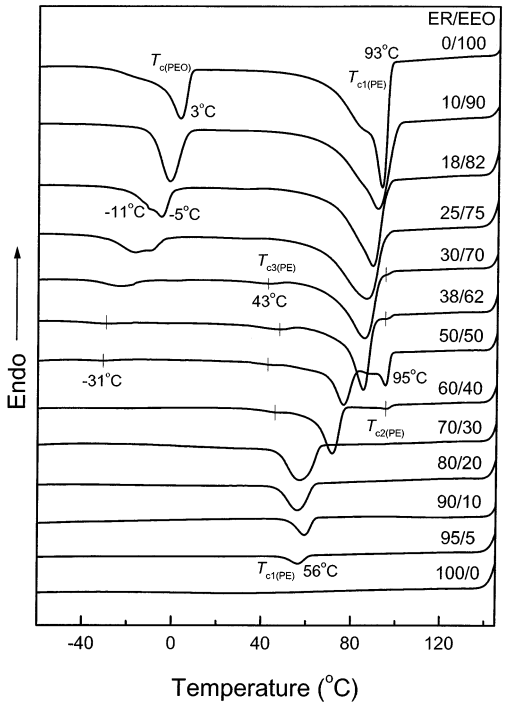

Figure 11. Crystallization curves of the MDA-cured ER/EEO blends during the cooling at −20 °C/min.

is expected for systems with a positive (endothermic) enthalpy of mixing. Miscibility between the components has recently been observed only in a few cases for cross-linked blends with hydrogen-bonding interactions.[8] It has been shown that the miscibility of an ER with a linear polymer is very dependent on the nature of curing agent.[8−10,24,25] PEO was found to be completely miscible with both DGEBA and aromatic diamine-cured ERs, including MDA-cured ER.[9,10]

The samples of all the MDA-cured ER/EEO blends were subjected to DSC measurement. Figure 10 shows DSC thermogams of the second scan of the MDA-cured ER, EEO, and the MDA-cured ER/EEO blends. The EEO diblock copolymer exhibits two obvious melting points, $T_{m(PEO)} = 23$ °C and $T_{m(PE)} = 106$ °C, attributable to the crystalline PEO blocks and the crystalline PE blocks, respectively. For the ER/EEO blends with EEO content up to 40 wt %, no melting peak for the PEO blocks appears. DSC thermogams of the first scan (not presented here for brevity) of the as-prepared MDA-cured ER/EEO blends with EEO content up to 40 wt % also did not display melting peak for the PEO blocks. This implies that the PEO blocks of the EEO copolymer are completely dissolved in the cured ER matrix for these blends. It can also be seen from Figure 10 that melting peak of PE blocks, $T_{m(PE)}$, remains little affected in the blends even with EEO content down to 5 wt %, consistent with the immiscibility between PE blocks and the ER matrix. It is interesting to notice that there is a small melting peak at 44 °C responsible for the PEO blocks. This peak was more profound, resulting in the appearance of a double melting peak of PEO blocks for the pure EEO as well as for the 10/90 ER/EEO blend in DSC thermograms of the first scan (not shown here). By conducting the DSC measurements of the first scan at different heating rates and with different start temperatures, it was shown that the appearance of this small peak is due to recrystallization of PEO blocks and the subsequent melting.

The MDA-cured ER displays a glass transition, $T_{g(ER)} = 177$ °C which shifts down to lower temperature with increasing EEO content up to 20 wt % and eventually disappears at higher EEO content. This result indicates that the PEO blocks and the ER matrix are miscible or at least partially miscible at these compositions. However, the reduction in T_g of the cured blends can result from a combination of two plasticization effects: internal and external. The dilution effect of the EEO component can result in a reduction in cross-linking density of the network and hence a reduction in its T_g.

Figure 11 shows DSC thermograms of the cooling scan for the cured ER/EEO blends at a cooling rate of −20 °C/min from 150 °C. All the samples were molten at 150 °C for 2 min prior to the cooling scan. The pure EEO copolymer displays a crystallization peak, $T_{c(PEO)}$, at 3 °C, attributable the crystallization of the PEO blocks. This crystallization peak, $T_{c(PEO)}$, shifts to lower temperatures in the blends with increasing ER content. The overall crystallization rate of PEO block of EEO copolymer in the cured blends decreases substantially with increasing ER content, which can be ascribed to the much higher T_g of the MDA-cured ER (177 °C) compared to that of PEO (ca. −60 °C).[10,24,25] Figure 11 illustrates that the 18/82 ER/EEO blend displays another crystallization exotherm at −11 °C beyond the crystallization peak at −5 °C. It is known that PEO can crystallize by either heterogeneous or homogeneous nucleation.[26] The appearance of the two crystallization exotherms of the 18/82 ER/EEO blend can be attributed to sequential heterogeneous and homogeneous nucleation. Initially, crystallization is induced by heterogeneous nucleation starting from −5 °C during the cooling scans. The crystallization rate of PEO block in the 18/82 ER/EEO blend is very slow, and the number of heterogeneous nuclei is small. Consequently, the crystallization process is not completed when the temper-

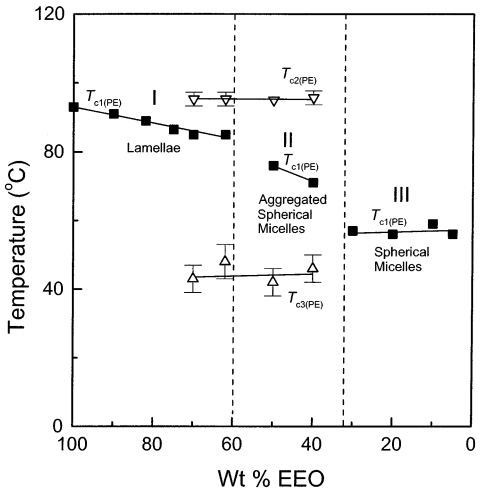

Figure 12. Crystallization temperatures of the PE blocks of the MDA-cured ER/EEO blends during the cooling scan. The plot of the major crystallization temperature, $T_{c1(PE)}$, of the PE blocks as a function of EEO content shows three regimes of crystallization kinetics corresponding precisely to the three morphological regimes.

ature reaches about −11 °C where homogeneous nucleation starts after formation of primary nuclei by the PEO block chains. The crystallization of the PEO blocks by homogeneous nucleation gradually becomes dominant for the blends with increasing ER content from 25 to 50 wt %. For the 50/50 ER/EEO blend, this crystallization peak becomes very small and shifts down to −31 °C, indicating a reduced crystallization rate. There is no crystallization exotherm of the PEO blocks during the cooling scan for the blends containing 40 wt % or less EEO. The crystallization behavior of the epoxy-miscible PEO blocks in the blends is as expected for crystallizable/miscible blends.

The pure EEO copolymer displays a major crystallization peak for the PE blocks, $T_{c1(PE)}$, at 93 °C, which does not remarkably shift to lower temperatures in the blends with EEO content down to 62 wt %, but then drops substantially to lower temperatures at 50 and 40 wt % EEO compositions. Finally, it reaches to almost a constant temperature when the EEO content is further reduced to 30 wt % and less. This peak does not disappear even in the blend containing as little as 5 wt % EEO. Besides, a small crystallization peak or shoulder, $T_{c2(PE)}$, appears on the right side (ca. 95 °C) for the blend containing 70−40 wt % EEO, indicating that the minority of crystallization was performed at an enhanced rate. This phenomenon suggests that the ER-rich phase that is separated out to some extent can act as a nucleation agent in these blends. Another small crystallization peak, $T_{c3(PE)}$, appears on the left side (40−50 °C) for the blends containing 70−40 wt % EEO, indicating that the crystallization of a small amount of PE blocks was performed at an greatly reduced rate in the blends. We will see below that this small crystallization peak, $T_{c3(PE)}$, can be attributed to the crystallization of the PE blocks confined in the individual spherical micelles that still exist in these blends. Crystallization of the PE blocks can be greatly slowed under the nanoscale confined environments.

Figure 12 summarizes crystallization temperatures of the PE blocks of the cured ER/EEO blends during the cooling scan as a function of the blend composition. A higher crystallization temperature corresponds to a faster crystallization rate. It is noted that the plot of the major crystallization temperature, $T_{c1(PE)}$, of the PE blocks as a function of EEO content shows three regimes of crystallization kinetics. In regime I, the crystallization temperature, $T_{c1(PE)}$, decreases very slowly with EEO content down to 62 wt %, and there is a linear relationship between the $T_{c1(PE)}$ and the blend composition. However, it drops discontinuously to low temperatures for the blends containing 50 and 40 wt % EEO (regime II). $T_{c1(PE)}$ decreases faster with decreasing EEO content in regime II than in regime I. Finally, $T_{c1(PE)}$ further drops remarkably to an even lower temperature for the blend containing 30 wt % EEO and remains almost unchanged for the blends containing 30−5 wt % EEO (regime III). This result shows that the kinetics and mechanism of crystallization of the PE blocks in the three regimes must be different. The PE blocks crystallized in the blends within three obviously different nanoscale confined environments. It will be interesting to notice that these three regimes of crystallization kinetics correspond respectively to three morphological regimes at nanoscales. In regime I, the blends show a semicrystalline microphase-separated lamellar morphology. In regime II, the blends display phase morphology of aggregated spherical micelles with some characteristic of bicontinuous microphase structure. In regime III, the blends exhibit phase morphology of spherical micelles. There exist parallel transitions of crystallization kinetics with microphase morphology. This is the first time that this phenomenon has been revealed in nanostructured thermoset blends.

Crystallization of block copolymers within nanoscale confined microdomains has recently been studied in crystalline-amorphous diblock copolymers[27−32] as well as in diblock copolymer/homopolymer blends.[33,34] It has been shown that crystallization of crystallizable blocks for crystalline−amorphous diblock copolymers can be efficiently confined within nanoenvironments when the amorphous blocks vitrify prior to the crystallization. Nucleation in diblock copolymers and their homopolymer blends within the nanoscale confined microdomains is principally homogeneous as the macroscopic impurities cannot be kept within the nanoscopic microdomains to act as the heterogeneous nuclei.[29,33,34] Analysis of the homogeneous nucleation rate in crystalline-amorphous diblock copolymers at a given temperature has been addressed by by Loo et al.[29] using the first-order kinetics. However, no study has involved with nanoscale confined crystallization in nanostructured block copolymer/thermoset blends. In the present study, the existence of parallel transitions between crystallization kinetics and microphase morphology in the nanostructured ER/EEO thermoset blends can be accounted for by the homogeneous nucleation controlled crystallization within the nanoscale confined PE microdomains. Provided the crystallization is homogeneous nucleation controlled and strictly restricted in the PE microdomains, the nucleation rate is directly proportional to the volume of the individual PE microdomain.[35] The volume of the microdomain follows the order of lamellae > aggregated spherical micelles > spherical micelles, so that the nucleation rate and hence the overall crystallization kinetics undergo corresponding transitions at the morphological transformations.

In regime I, for the blends with low ER content, only highly branched ER chain molecules and an imperfect network are actually formed. The insufficiently cured

ER molecules and the PEO blocks are miscible, forming one microphase with T_g much lower than $T_{m(PE)}$. Crystallization of PE blocks in the ER/EEO blends in regime I cannot be efficiently confined within the PE microdomains as the microphase composed of insufficiently cured ER and PEO blocks does not vitrify prior to the crystallization.[27] The crystallization process takes place through heterogeneous nucleation and completes prior to homogeneous nucleation. The crystallization is highly cooperative among the PE microdomains so that the crystal growth can propagate over a macroscopic scale comparable to spherulitic crystallization in homopolymer. Crystallization of the PE blocks in the blends in regime I is analogous to the common spherulitic crystallization in homopolymers. The crystallization mechanism is essentially identical with the conventional spherulitic crystallization with long-range crystal growth from the heterogeneous nuclei. It has been reported that long-range crystal growth can result in a highly interconnected lamellar morphology over a macroscopic scale and formation of spherulites in lamellar block copolymers[36] as well as in block copolymer/homopolymer blends.[37]

In regime II, the crystal growth is substantially restricted in the aggregated spherical micelles with characteristic of bicontinuity which are nearly two-dimensionally confined at nanoscales. The crystallization temperature, $T_{c1(PE)}$, decreases rapidly with decreasing EEO content. The undercooling is exceedingly enlarged with decreasing EEO content, indicating that the crystallization of the PE blocks in aggregated spherical micelles by homogeneous nucleation becomes dominant.[35] In regime III, the crystal growth is highly restricted in the spherical micelles that are three-dimensionally confined at nanoscales. The crystallization is largely confined within the individual spherical micelles. Because the crystal growth of the PE block within a spherical micelle cannot advance toward other spherical micelles, every PE spherical micelle needs to acquire a crystalline nucleus to initiate the crystallization within it. This is asserted by the extremely large undercoolings observed for all the blends in regime III. It is clear that the crystallization kinetics of the PE blocks in spherical micelles is homogeneous nucleation controlled, i.e., homogeneous nucleation is the rate-determining step in the crystallization.

It is also noticed that the small crystallization peaks, $T_{c3(PE)}$, for the blends at the mid-compositions of 70−40 wt % EEO are even lower than the crystallization temperature, $T_{c1(PE)}$, in the spherical micelles for the blends at the lowest compositions (30−5 wt % EEO). This result means that the small crystallization peaks, $T_{c3(PE)}$, can be attributed to the homogeneous nucleation controlled crystallization of the PE blocks in some individual spherical micelles that remain in these blends.

Conclusions

We have presented here the first example of self-organized thermoset blends with diblock copolymers consisting of a thermoset-miscible block and a crystallizable thermoset-immiscible block. All the MDA-cured ER/EEO blends do not show macroscopic phase separation, and the nanostructured thermoset blends can be obtained. The epoxy-immiscible PE blocks can form separate microdomains at nanoscales in the thermoset ER/EEO blends and crystallize within the nanoscale confined environments. For the nanostructured ER/EEO blends with EEO content up to 30 wt %, only the PE crystals with size on nanoscales can be formed; they are nanoscopically restricted within the individual spherical micelles. However, for the blends containing 40 and 50 wt % EEO, spherical micelles are highly aggregated. The PE dentritic crystallites with size of 2−5 μm in diameter were observed in the blend containing 50 wt % EEO and the blends with even higher EEO content were completely volume-filled with PE spherulites of size of 10−30 μm in diameter. Here we have shown there exist three regimes of crystallization kinetics of the PE blocks, corresponding precisely to three morphological regimes identified as follows: (1) the semicrystalline microphase-separated lamellae in the symmetric EEO diblock copolymer that are swollen in the blend with decreasing EEO content, followed by a structural transition to (2) aggregated spherical micellar phase morphology, and eventually (3) spherical micellar phase morphology at the lowest EEO contents. The semicrystalline morphology and crystallization kinetics have been shown to be greatly affected within the nanoscale confined environments. We have revealed the nanoscale confinement effect on the crystallization kinetics in nanostructured block copolymer/thermoset blends for the first time. This new phenomenon can be explained on the basis of homogeneous nucleation controlled crystallization within different nanoscale confined environments in nanostructured thermoset blends.

Acknowledgment. Q.G. would like to express his gratitude to the Alexander von Humboldt Foundation for awarding a Humboldt Research Fellowship.

References and Notes

(1) Hillmyer, M. A.; Lipic, P. M.; Hajduk, D. A.; Almdal, K.; Bates, F. S. *J. Am. Chem. Soc.* **1997**, *119*, 2749.
(2) Lipic, P. M.; Bates, F. S.; Hillmyer, M. A. *J. Am. Chem. Soc.* **1998**, *120*, 8963.
(3) Mijovic, J. S.; Shen, M.; Sy, J. W.; Mondragon, I. *Macromolecules* **2000**, *33*, 5235.
(4) Dean, J. M.; Lipic, P. M.; Grubbs, R. B.; Cook, R. F.; Bates, F. S. *J. Polym. Sci., Part B: Polym. Phys.* **2001**, *39*, 2996.
(5) Kosonen, H.; Ruokolainen, J.; Nyholm, P.; Ikkala, O. *Macromolecules* **2001**, *34*, 3046.
(6) Kosonen, H.; Ruokolainen, J.; Nyholm, P.; Ikkala, O. *Polymer* **2001**, *42*, 9481.
(7) Guo, Q.; Thomann, R.; Gronski, W.; Thurn-Albrecht, T. *Macromolecules* **2002**, *35*, 3133.
(8) Guo, Q. In *Polymer Blends and Alloys*; Shonaike, G. O., Simon, G., Eds.; Marcel Dekker: New York, 1999; Chapter 6, pp 155−187.
(9) Zheng, S.; Zhang, N.; Luo, X.; Ma, D. *Polymer* **1995**, *36*, 3609.
(10) Guo, Q.; Harrats, C.; Groeninckx, G.; Koch, M. J. H. *Polymer* **2001**, *42*, 4127.
(11) Strobl, G. *Acta Crystallogr.* **1970**, *A26*, 367.
(12) Trent, J. S.; Scheinbeim, J. I.; Couchman, P. R. *Macromolecules* **1983**, *16*, 589.
(13) Thomann, Y.; Thomann, R.; Bar, G.; Ganter, M.; Machutta, B.; Mülhaupt, R. *J. Microsc.* **1999**, *195*, 161.
(14) Hillmyer, M. A.; Bates, F. S. *Macromol. Symp.* **1997**, *117*, 121.
(15) Leibler, L. *Macromolecules* **1980**, *13*, 1602.
(16) Benoit, H.; Hadziioannou, G. *Macromolecules* **1988**, *21*, 1449.
(17) Mortensen, K. *J. Phys.: Condens. Matter. A* **1996**, *8*, 103.
(18) Kinning, D. J.; Thomas, E. L. *Macromolecules* **1984**, *17*, 1712.
(19) Schwab, M.; Stühn, B. *Phys. Rev. Lett.* **1996**, *76*, 924.
(20) Schwab, M.; Stühn, B. *J. Chem. Phys.* **2000**, *112*, 6461.
(21) Giunier, A.; Fournet, G. *Small-Angle Scattering of X-rays*; Wiley: New York, 1955.
(22) Ornstein, L. S.; Zernike, F. *Proc. Akad. Sci. Amsterdam* **1914**, *17*, 793.

(23) Percus, J. K.; Yevick, G. J. *Phys. Rev.* **1958**, *110*, 1.
(24) Guo, Q.; Peng, X.; Wang, Z. *Polym. Bull. (Berlin)* **1989**, *21*, 593.
(25) Guo, Q.; Peng, X.; Wang, Z. *Polymer* **1991**, *32*, 53.
(26) Wundlich, B. *Macromolecular Physics*; Academic Press: New York, 1976; Vol. 2, p 24.
(27) Hamley, I. W. *Adv. Polym. Sci.* **1999**, *148*, 113.
(28) Weimann, P. A.; Hajduk, D. A.; Chu, C.; Chaffin, K. A.; Brodil, J. C.; Bates, F. S. *J. Polym. Sci., Part B: Polym. Phys.* **1999**, *37*, 2053.
(29) Loo, Y. L.; Register, R. A.; Ryan, A. J. *Phys. Rev. Lett.* **2000**, *84*, 4120.
(30) Loo, Y. L.; Register, R. A.; Ryan, A. J. *Macromolecules.* **2002**, *35*, 2365.
(31) Zhu, L.; Cheng, S. Z. D.; Calhoun, B. H.; Ge, Q.; Quirk, R. P.; Thomas, E. L.; Hsiao, B. S.; Yeh, F.; Lotz, B. *J. Am. Chem. Soc.* **2000**, *122*, 5957.
(32) Zhu, L.; Calhoun, B. H.; Ge, Q.; Quirk, R. P.; Cheng, S. Z. D.; Thomas, E. L.; Hsiao, B. S.; Yeh, F.; Liu, L.; Lotz, B. *Macromolecules* **2001**, *34*, 1244.
(33) Chen, H. L.; Hsiao, S. C.; Lin, T. L.; Yamauchi, K.; Hasegawa, H.; Hashimoto, T. *Macromolecules* **2001**, *34*, 671.
(34) Chen, H. L.; Wu, J. C.; Lin, T. L.; Lin, J. S. *Macromolecules* **2001**, *34*, 6936.
(35) Cormia, R. L.; Price, F. P.; Turnbull, D. *J. Chem. Phys.* **1962**, *37*, 1333.
(36) Floudas, G.; Tsitsilianis, C. *Macromolecules* **1997**, *30*, 4381.
(37) Sakurai, K.; MacKnight, W. J.; Lohse, D. J.; Schultz, D. N.; Sissano, J. A. *Macromolecules* **1994**, *27*, 4941.

MA0340154